Regional Ultrahigh-Resolution Rescan in a Clinical Whole-Body CT Scanner Using a Contact Detector Insert

Thomas C. Larsen[1], Eric E. Bennett[1], Dumitru Mazilu[1], Marcus Y. Chen[2], and Han Wen[1]

[1]Imaging Physics Laboratory, Biochemistry and Biophysics Center and [2]Cardiovascular Branch, National Heart, Lung and Blood Institute, National Institutes of Health, Bethesda, MA

Corresponding Author:
Han Wen, PhD
Imaging Physics Laboratory, Biochemistry and Biophysics Center, National Heart, Lung and Blood Institute, NIH, Bethesda, MD 20892-1061;
E-mail: wenh@nhlbi.nih.gov

Key Words: CT re-scan, ultrahigh resolution, ultralow dose, contact detector insert, tomosynthesis, hybrid CT

Abbreviations: Computed tomography (CT), contact detector inserts (CDIs), high-resolution CT (HRCT), axial HRCT (a-HRCT)

ABSTRACT

Ultrahigh-resolution, low-dose rescans in a region of interest following a general screening computed tomography (CT) scan is motivated by the need to reduce invasive tissue biopsy procedures in cancer screening. We describe a new method to meet the conflicting demands of ultrahigh resolution, high-speed and ultralow-dose, and the first proof-of-concept experiment. With improving detector resolution, the limiting factor for the system resolution of whole-body CT scanners shifts to the penumbra of the source focal spot. The penumbra unsharpness is minimized by inserting flat-panel detector(s) that are in direct contact with the body. In the hybrid system, the detector insert and the CT detector acquire data simultaneously, whereby the standard CT images give the position and orientation of the detector insert(s) as needed for tomosynthesis reconstruction. Imaging tests were performed with a compact photon-counting detector insert on resolution targets of both high- and low-contrast as well as a mouse specimen, all inside a body phantom. Detector insert tomosynthesis provided twice the resolution of the CT scanner alone at the same dose concentration. The short 2-cm beam collimation of the tomosynthesis rescan gave an effective dose equivalent to 6% of an average CT scan in the chest or abdomen.

INTRODUCTION

Driven by the desire to reduce invasive biopsy procedures in cancer screening, technologies are being rapidly developed to provide ultrahigh resolution in a limited region of interest, which allows a detailed rescan of a suspect area revealed by a standard scan while the patient is still in the computed tomography (CT) scanner (1–3). The CT system resolution is influenced by the detector resolution, the size of the x-ray tube focal spot and the local dose concentration (CTDIvol). To realize a high-resolution rescan in standard whole-body CT scanners, protocols have been developed to increase the CTDIvol by multiple fold in a short Z length to provide high-resolution locally (3); further improvement comes with the recent implementation of ultrahigh-resolution multirole detectors in whole-body CT scanners (1) and high-resolution photon-counting detectors (2). With such detectors, the limiting factor of resolution becomes the focal spot penumbra, namely, blurring of the images by the finite size of the x-ray source spot. One approach to overcome the focal spot limit is a system design that includes a micro focus source on an inner ring inside the scanner bore. But it has yet to be realized owing to major engineering changes to the CT system.

On the other hand, because the focal spot penumbra is proportional to the distance between the object and the image plane, contact radiography and mammography minimize the distance to achieve excellent resolution with relatively large focal spots. Based on this idea, we describe an alternative method to break the focal spot limitation in clinical whole-body CT scanners, and the first experimental demonstration. The general idea is to add detector inserts inside the CT bore which are in direct contact with the body, for example, on the patient bed (Figure 1A). In this configuration, the focal spot penumbra on the detector insert is reduced by several fold when compared to the existing CT detector in the rotating gantry (Figure 1B). In operation, the detector inserts are mechanically shifted out of view during the standard CT scan, and shifted into the bore for the high-resolution rescan. A unique synergy of this hybrid system is the simultaneous data acquisition by the detector insert and the CT detector during the high-resolution rescan: images from the CT detector show the position and orientation of the detector insert inside the bore, which is necessary information for the tomosynthesis reconstruction of the data collected by the Detector Insert.

© 2019 The Authors. Published by Grapho Publications, LLC This is an open access article under the CC BY-NC-ND license (http://creativecommons.org/licenses/by-nc-nd/4.0/).
ISSN 2379-1381 https://doi.org/10.18383/j.tom.2019.00002

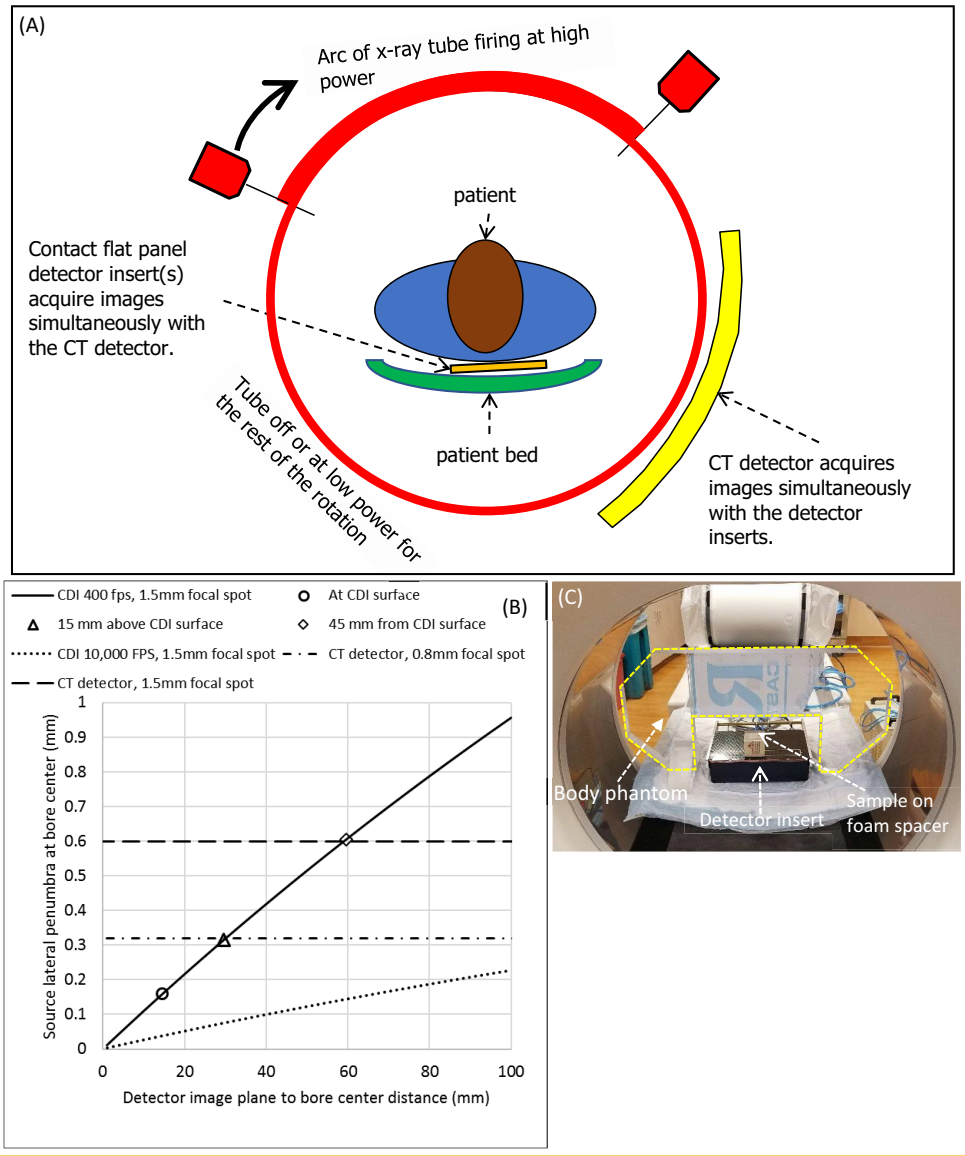


Figure 1. Concept of the contact detector insert (CDI) and experimental setup. In the schematic of a hybrid computed tomography (CT) system, the x-ray tube is switched on over part of the gantry rotation for tomosythesis by the CDI. The CT detector simultaneously acquires data to provide positional information of the CDI (A). Estimated x-ray tube focal spot penumbras at the bore center for the CDI and the CT detector, for the Toshiba Aquilion One Genesis scanner, accounting for gantry rotation (B). The circle, triangle and diamond mark actual experiments. Dotted line is for a hypothetical high-speed detector insert. Dashed line is for the detector of the CT scanner operating at high-power/large focal spot mode. Dash-dotted line is for the CT scanner operating at low-power/small focal spot mode, which is the mode that provided the best resolution in standard HRCT scans. The experimental setup includes an acrylic body phantom outlined in dashed line, the photon-counting detector insert, and various resolution phantoms and samples (C).

The method was tested in a clinical whole-body CT scanner (Figure 1C). The detector insert was a flat-panel photon-counting detector placed on the patient bed. An acrylic body phantom that simulated the attenuation of an adult torso was used in all imaging tests to provide realistic signal levels. Images of resolution targets inside the body phantom resolved 0.2-mm-diameter holes in a square matrix of 0.4-mm pitch in a 0.30-second scan, in comparison to the 0.5-mm holes/1.0-mm pitch by the CT scanner alone at the same dose concentration CTDIvol in a 0.6-second scan. Images of a mouse specimen inside the body phantom were also compared.

Regarding the limitations of this approach, a technical bottleneck is the 400 FPS imaging speed of the flat-panel photon-counting detector, which is $<1/20$th the speed of a clinical CT detector. It meant that image blurring in the lateral direction is dominated by the movement of the x-ray focal spot. This is because as the gantry rotates, the travel distance of the focal spot during the acquisition of a single projection image is several times the size of the spot. This point was verified experimentally. Other limitations are inherent to tomosynthesis, including out-of-plane shadowing artifacts, an-isotropic image resolution, and lack of a measure of the absolute CT density in Hounsfield units.

Looking into the future, while clinical whole-body CT scanners continually achieve smaller focal spot size and better detector resolution, focal spot size penumbra continues to be a limiting factor in system resolution. For example, the latest photon-counting detectors provide resolutions better than 50 μm (4), while the progress of focal spot size lags behind, reaching 0.4–0.5 mm, currently at low power settings (https://www.itnonline.com/content/canon-medical-systems-aquilion-precision-ct-receives-fda-clearance). Therefore, contact detector inserts (CDIs) should continue to provide an extra boost of resolution in a targeted rescan of a region of interest in future whole-body scanners. Future development directions include more sophisticated and customized image reconstruction methods for the tomosynthesis rescan, and faster photon-counting detector inserts to reduce blurring

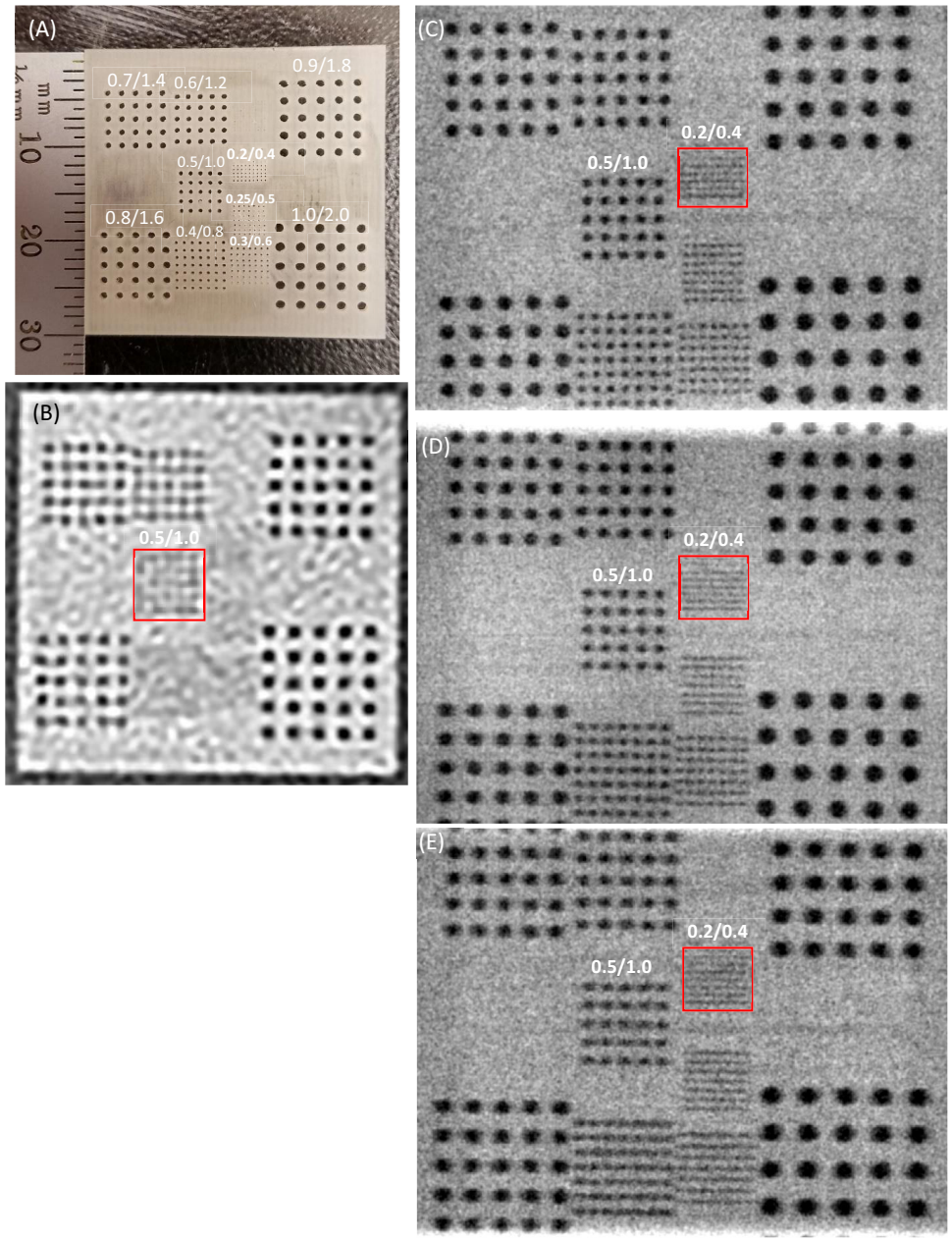


Figure 2. Comparison of the CT image and CDI tomosynthesis images of a resolution card, taken at the same CTDIvol inside the body phantom. The tomosynthesis images were taken at various sample-to-detector distances. A picture of the 3D printed resolution card of 1.0 mm of thickness, consisting of matrices of air holes (A). The labels denote the hole diameter/center-to-center spacing of the hole matrices. The CT scan resolved the 0.5-mm hole matrix (red box) (B). The CDI tomosythesis scan resolved the 0.2-mm hole matrix (red box) when the card was place on the surface of the detector (15 mm from the image plane within the detector) (C). When the resolution card was elevated to 15 mm above the detector surface (30 mm from the image plane) with a foam spacer, the CDI image was blurred in the horizontal direction due to focal spot travel over the image acquisition time, and resolved only the 0.2-mm hole matrix vertically (red box) (D). The resolution card was further elevated to 45 mm above the detector surface (60 mm from the image plane), and further horizontal blurring was seen due to focal spot travel (E).

due to gantry rotation. These will be elaborated in the Discussion section.

METHODOLOGY

The body phantom was made of solid acrylic (Figure 1C). It provided a ≥15-cm path length of attenuation through the acrylic material for all scans to simulate that of an adult body.

Two resolution phantoms were imaged inside the body phantom (Figure 1C). The first was a 3D printed polymer card of 1 mm thickness (Figure 2A) that contained matrices of air holes of decreasing diameter and increasing density. The CT attenuation coefficient of the polymer material was 130 HU at 120 kV. The second, a low-contrast card, was also 3D printed to the same dimensions, but with the holes filled with wax. The CT attenuation coefficient of the wax was −105 HU, or a 235 HU contrast from the surrounding polymer.

A mouse specimen was also imaged. The specimen was fixed in 10% formalin in a centrifuge tube, and the tube was placed horizontally on the surface of the detector insert, inside the body phantom.

Both the CDI tomosynthesis scan and the high-resolution CT scan used the axial (cone beam) mode of the scanner with a static patient bed, to provide the highest dose concentration for a given beam collimation and scan time, which maximizes the signal-to-noise ratio (3).

The contact detector insert was a photon-counting detector (Xcounter Thor Model, Direct Conversion AB, Danderyd, Sweden) of 256 × 2048 pixel matrix and 0.1-mm pixel pitch, 400 frames/s acquisition rate in a 16-bit mode, and single energy threshold of 25 keV. The CT scanner parameters for the tomosynthesis scan were axial (cone beam) mode 120 kV/700 mA (large focal spot mode), 1.5 s/turn rotation speed, data acquisition over the top 72° arc of

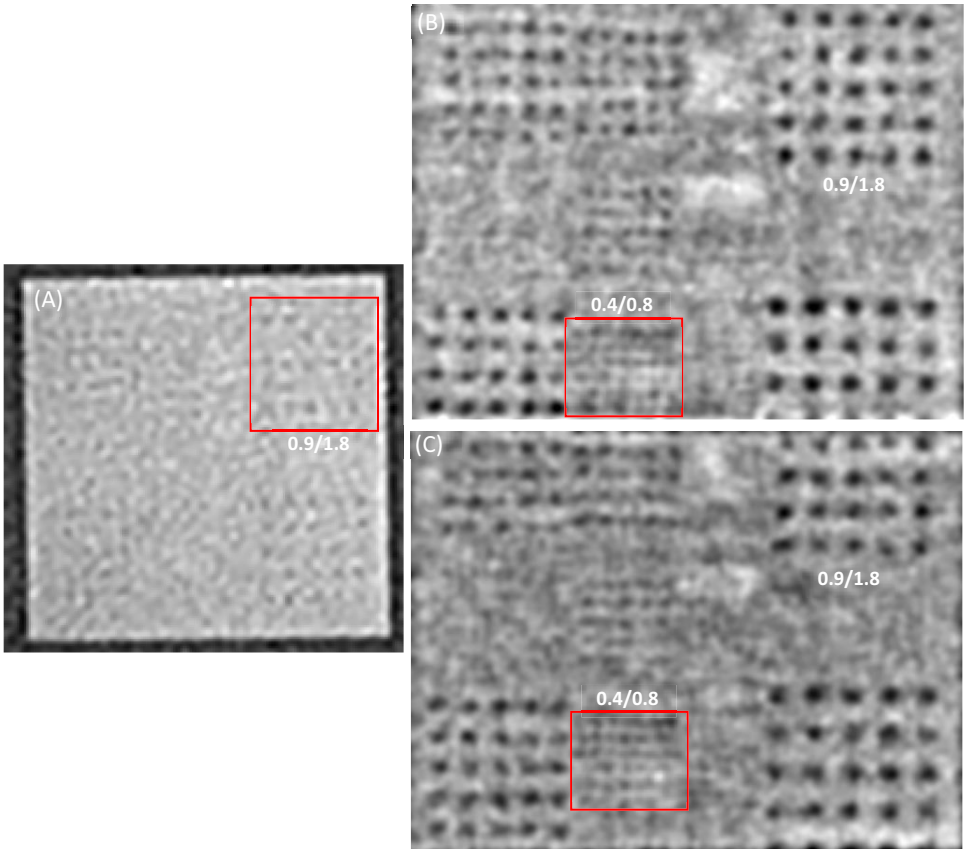


Figure 3. Comparing CT and CDI tomosynthesis images of a low-contrast resolution card acquired at the same CTDIvol inside the body phantom. The phantom was a 1.0-mm-thick 3D printed polymer card with an identical pattern to the card in Figure 2, but with the holes filled with wax to provide a 235 HU contrast between the polymer and the wax. The CT image detected some of the 0.9-mm diameter holes (red box). The label is hole diameter/center-to-center spacing (A). The CDI tomosynthesis image resolved the 0.4-mm hole array (red box) when the card was placed on the surface of the detector (sample-to-image distance of 15 mm) (B). In the CDI tomosynthesis image of the card which was placed at 45 mm above the detector surface with a foam spacer (sample-to-image distance of 60 mm), the same resolution was retained (C).

gantry rotation in 0.3 seconds and 210 mAs, beam collimation of 2 cm and CTDIvol of 15.2 mGy. The image plane within the detector, which is the semiconductor conversion layer, lies at 14.6 mm below the surface of the detector. The resolution cards were placed either directly on the surface of the detector, corresponding to a distance of 14.6 mm to the image plane, or on 15- and 45-mm-thick foam spacers, corresponding to a distance of 29.6 mm and 59.6 mm to the image plane. A basic filtered back-projection tomosynthesis image reconstruction was used to reconstruct images at 0.05-mm pixel size at various depths from the surface of the detector.

For the axial high-resolution CT (HRCT) image acquisition, the CDI was removed. The resolution cards were positioned in the axial plane inside the body phantom for best resolution. The mouse sample was placed directly on the bed of the scanner. All samples were positioned at the isocenter of the bore. Scan parameters were axial cone beam mode of 120 kV/350 mA (small focal spot mode) and 210 mAs (0.6 seconds of rotation time), beam collimation of 20 × 0.5 mm (3), and CTDIvol of 15.2 mGy. Images were reconstructed with the FC52 kernel, in-plane pixel size of 0.25 mm, slice center-to-center spacing of 0.25 mm, and slice thickness of 0.5 mm. This reconstruction setting was found to provide the best resolution.

RESULTS

Figure 2, B–E compares the axial HRCT (a-HRCT) and CDI tomosynthesis images of the high-contrast (1130 HU) resolution card inside the body phantom, which were acquired at the same dose concentration (CTDIvol). For the a-HRCT image (Figure 2B), the reconstruction pixel size of 0.25 mm was found visually to give the best resolution. The smallest resolved features were the matrix of 0.5 mm holes. The CDI tomosynthesis image of the resolution card resolved the 0.2-mm hole matrix when the card was placed directly on the detector (Figure 2C). When the card was placed at 15 mm and 45 mm above the detector surface, CDI tomosynthesis could only resolve the 0.2-mm holes vertically while they were horizontally burred (Figure 2, D and E). This was caused by the 6.3-mm travel of the x-ray focal spot over the acquisition time per frame, which led to a growing lateral penumbra of the focal spot with increasing distance from the detector, as illustrated in Figure 1B.

Figure 3 compares the a-HRCT and CDI tomosynthesis images of the low-contrast (235 HU) resolution card at the same CTDIvol level. The a-HRCT image showed some of the 0.9-mm wax dots (Figure 3A); the CDI tomosynthesis images resolved the matrix of 0.4-mm wax dots (Figure 3B) when the card was placed on the detector surface or elevated at 45 mm from the surface.

Figure 4 compares the a-HRCT and CDI tomosynthesis images of the mouse specimen, again at the same dose concentration level. Two different horizontal sections are shown. The CDI image resolved the bone structures at higher resolution such as the individual ribs, and also visualized structures in the nose and head and the abdominal cavity which were not visible by a-HRCT.

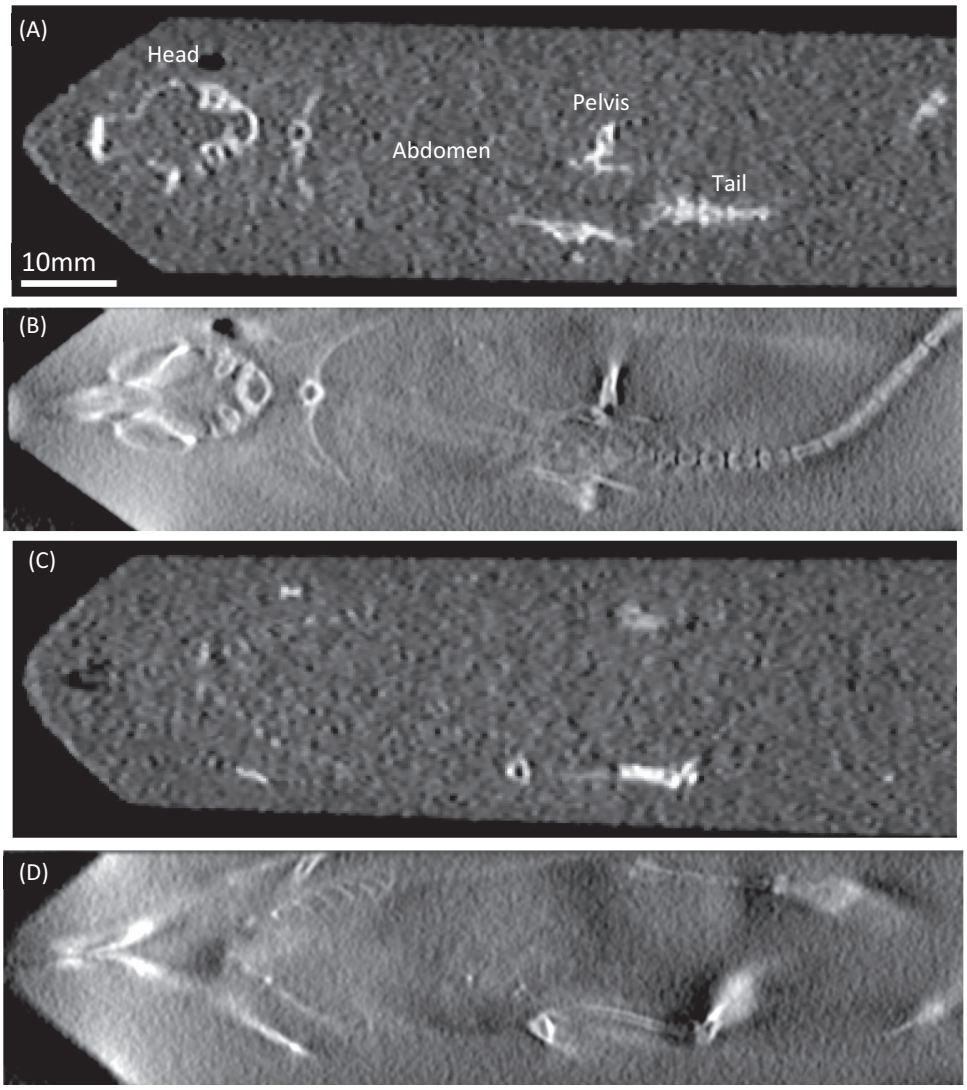


Figure 4. Comparing CT and CDI tomosythesis images of a formalin-fixed mouse specimen placed in the body phantom. The specimen is fixed in formalin in a centrifuge tube. The same CTDIvol of 15.2 mGy was used. (A) and (C) are CT scan coronal sections. (B) and (D) are the CDI images of the same locations. The resolution of the bone structures is higher in the CDI images; structures in the nose and head and the abdominal cavity become visible in the CDI images.

DISCUSSION

As a first test, this study shows that a contact detector insert in a whole-body CT scanner achieves ultrahigh resolution in a 0.3-second scan under a realistic level of attenuation by an adult body, in a zone near the detector. The depth of the zone is currently limited by the frame rate of the detector. The principle for high resolution is similar to that of contact radiography, and the concept in general is similar to surface coils in body MRI, which provide high sensitivity and resolution near the coils. When comparing the results of the high- versus low-contrast resolution cards in the presence of the body phantom attenuation, it was clear that the resolution decreases with lower contrast, although the CDI tomosynthesis scan maintains a factor of two resolution relative to the CT scanner itself at the same dose.

For comparison, a recent Toshiba Aquilion family CT scanner has an ultrahigh resolution mode of 0.25-mm pixel pitch at the bore center, which was shown to resolve 0.12-mm-wide slits (1). However, this was shown in a resolution target alone without the attenuation of a body phantom, and at 2.4 times the dose concentration of this study (CTDIvol of 36.6 mGy vs 15.2 mGy). More significantly, it required low power output of the x-ray tube to maintain a smaller focal spot size, leading to scan times of several seconds compared to the 0.3-second scan of this study. Scan time is a significant factor for ultrahigh resolution, as subtle motion and drift of the body blur the images over time. Radiation dose is also a significant factor for rescans, as it adds dose onto the standard scan. Using the dose-length-product (DLP = 30.3 mGy*cm) reported by the scanner in this study, we estimate that the added effective dose of the CDI tomosynthesis rescan in the chest and abdomen to be 0.42 mSv and 0.45 mSv on average (5), which is equivalent to 6% of a standard chest or abdomen CT scan (https://www.radiologyinfo.org/en/info.cfm?pg=safety-xray). This level of added dose should not impose significant burden on the patient, and it should also allow rescans of several regions in certain cases. The weakness of the CDI method, as mentioned in the Introduction section, involves inherent limitations of tomosynthesis, including out-of-plane shadows, anisotropic resolution, and lack of absolute CT density measurements.

The mass of the body phantom was mostly on 3 sides of the resolution targets to simulate the position of the body above the contact detector insert. This asymmetric disposition did not have adverse effects on the image quality of the standard CT scans as long as the resolution targets were positioned at the center of the bore: the same image quality and resolution were attained when

compared with the same a-HRCT scans on a standard body phantom with resolution inserts from a previous study (3).

Further developments are envisioned in both hardware and software. For software, this study used basic reconstruction procedures without any artifact reduction measures. A significant part of the on-going work is the improvement of the reconstruction methods in both algorithms and computation speed. Advanced tomosynthesis reconstruction methods that are being developed for other applications such as digital breast tomosynthesis [see reference (7) for a review] may be considered to see whether they are suitable for this application. Depending on the location of the region of interest within the body for the rescan, the influence of strongly attenuating structures such as bone and implanted devices may vary widely. Therefore, the reconstruction method and the placement of the contact detector insert should be adaptable to the location of the rescan.

For hardware, multiple detectors can be inserted to conform to the surface of the body for optimal coverage of a targeted internal region or several regions. The speed of compact photon-counting detectors is improving and can be expected to match that of CT detectors in a few years, thereby increasing the depth of the high-resolution zone as illustrated by the dotted line in Figure 1B of a hypothetical detector insert of 10,000 fps speed. A recent development is flexible x-ray detectors of high sensitivity using hybrid organic–inorganic materials (6), which may lead to contact detector inserts that can bend and conform to the shape of the body, much like the surface coils of MRI scanners. Whether using multiple detectors or bendable detectors, the exact geometry of the detector inserts during each scan need to be determined for tomosynthesis reconstruction. Therefore, the simultaneous image acquisition by the CT scanner itself becomes indispensable for this purpose.

ACKNOWLEDGMENTS

We are grateful to Joel Moss of NHLBI for discussions, to Shirley Rollison and Xi Tao of NHLBI for their assistance with the scans, and to the NHLBI Animal Surgery and Resource Core for the specimen. We are grateful to Christer Ullberg and Hamdan Amin of Xcounter for their assistance with the detector insert. This work is supported by the Intramural Research Program of NIH, National Heart, Lung, and Blood Institute.

Disclosures: Han Wen is the inventor of a patent application for this technology by the National Institutes of Health.

Conflict of Interest: The authors have no conflict of interest to declare.

REFERENCES

1. Kakinuma R, Moriyama N, Muramatsu Y, Gomi S, Suzuki M, Nagasawa H, Kusumoto M, Aso T, Muramatsu Y, Tsuchida T, Tsuta K, Maeshima AM, Tochigi N, Watanabe S, Sugihara N, Tsukagoshi S, Saito Y, Kazama M, Ashizawa K, Awai K, Honda O, Ishikawa H, Koizumi N, Komoto D, Moriya H, Oda S, Oshiro Y, Yanagawa M, Tomiyama N, Asamura H. Ultra-high-resolution computed tomography of the lung: image quality of a prototype scanner. Plos One 2015;10:e0137165.
2. Pourmorteza A, Symons R, Henning A, Ulzheimer S, Bluemke DA. Dose efficiency of quarter-millimeter photon-counting computed tomography first-in-human results. Invest Radiol. 2018;53:365–372.
3. Larsen TC, Gopalakrishnan V, Yao JH, Nguyen CP, Moss J, Wen H. Optimization of a secondary VOI scan for lung imaging in a clinical CT scanner. J Appl Clin Med Phys. 2018;19:271–280.
4. Hosono R, Kawabata T, Hayashida K, Kudo T, Ozaki K, Teranishi N, Hatsui T, Hosoi T, Watanabe H, Shimura T. Advancement of X-ray radiography using microfocus X-ray source in conjunction with amplitude grating and SOI pixel detector, SOPHIAS. Opt Express. 2018;26:21044–21053.
5. Christner JA, Kofler JM, McCollough CH. Estimating effective dose for CT using dose-length product compared with using organ doses: consequences of adopting International Commission on Radiological Protection publication 103 or dual-energy scanning. AJR Am J Roentgenol. 2010;194:881–889.
6. Thirimanne HM, Jayawardena KDGI, Parnell AJ, Bandara RMI, Karalasingam A, Pani S, Huerdler JE, Lidzey DG, Tedde SF, Nisbet A, Mills CA, Silva SRP. High sensitivity organic inorganic hybrid X-ray detectors with direct transduction and broadband response. Nat Commun. 2018;9:2926.
7. Sechopoulos I. A review of breast tomosynthesis. Part II. Image reconstruction, processing and analysis, and advanced applications. Med Phys. 2013;40:014302.